Chapter 4

Residual Stress in Friction Stir Welding and Laser-Assisted Friction Stir Welding by Numerical Simulation and Experiments

Caterina Casavola, Alberto Cazzato and
Vincenzo Moramarco

Additional information is available at the end of the chapter

http://dx.doi.org/10.5772/intechopen.72271

Abstract

The friction stir welding (FSW) has become an important welding technique to join materials that are difficult to weld by traditional fusion welding technology. In this technique, the material is not led to fusion, and the joint is the result of the rotation and movement along the welding line of the tool that causes softening of material due to frictional heat and the stirring of the same. In FSW, the temperature does not reach the fusion value of the materials, and this helps to decrease the residual stress values. However, due to the higher force involved in the weld and, thus, the rigid clamping used, the residual stresses are not low in general in this technique. As the presence of high residual stress values influences the post-weld mechanical properties, e.g. fatigue properties, it is important to investigate the residual stress distribution in the FSW welds. In this chapter, two numerical models that predict temperatures and residual stresses in friction stir welding and laser-assisted friction stir welding will be described. Experimental measurements of temperatures and residual stress will be carried out to validate the prediction of the models.

Keywords: friction stir welding, laser-assisted friction stir welding, residual stress, thermography, X-ray diffraction

1. Introduction

Since 1991, when the process was initially developed, friction stir welding (FSW) has become a promising welding method for joining materials that would otherwise be hardly weldable by means of the conventional welding technology [1]. This important advantage is mainly due to the FSW nature of being a solid-state welding process. In fact, the material is not

fused, and the welding process is the result of the tool rotation and movement along the welding line that causes softening of material due to frictional heat and the stirring of the same. In FSW, the temperature does not reach the fusion value of the materials, and this helps to decrease the residual stress values. However, due to the higher force involved in the weld and, thus, the rigid clamping used, the residual stresses are not low in general in this technique. The constraints avoid the contraction of the materials during cooling in both longitudinal and transverse directions, thereby resulting in generation of longitudinal (parallel to welding direction) and transverse stresses (normal to welding direction). As the presence of high residual stress values influences the post-weld mechanical properties, e.g. fatigue properties, it is important to investigate the residual stress distribution in the FSW welds. Some studies have been carried out on residual stresses in FSW [1, 2–5]. In most of these, some similar conclusions can be highlighted. First, the residual stresses in FSW welds are lower than those generated during fusion welding, but they are not negligible at all. The low residual stress in the FSW welds has been attributed to the lower heat input during FSW and recrystallization accommodation of these stresses. Second, the transverse stresses are lower than the longitudinal ones, independent on tool rotation rate, traverse speed and pin diameter. Third, the distributions of the transverse and longitudinal residual stresses show an "M"-like trend across the welded joint. Moreover, in the advancing side, there is a higher residual stress peak [1].

This chapter will describe the temperature fields and residual stresses in both FSW and laser-assisted friction stir welding (LAFSW), evaluated by means of experimental measurements and finite element analysis. Two numerical models will be developed and validated on the experimental results of temperatures and residual stresses. Furthermore, besides a deeper knowledge of FSW, these numerical simulations have also the aim to guide the development of the process through the research of optimal parameters minimising the amount of trial and error.

2. The friction stir welding process

The FSW main idea is very simple. A rotating tool is inserted into the plates to be welded, and while rotating, it is moved along the welding line (**Figure 1**).

During the FSW process, the material undergoes a severe plastic deformation at elevated temperature. This generates a fine and equiaxed recrystallized grain structure that produces good mechanical properties [1, 6].

2.1. Process

The welding process is divided into four main steps: rotating, plunge and dwell, translation and exit. The tool starts to rotate before the plunge phase (**Figure 2a**). During the plunge phase, the tool penetrates the material, and subsequently, it is held in position for a few seconds while still rotating (**Figure 2b**). This phase is called dwell time, and the aim of this step is to heat and thus soften the material before welding. Then the tool moves along the joint line carrying out the weld (**Figure 2c**). Finally, the tool is pulled out from the material (**Figure 2d**).

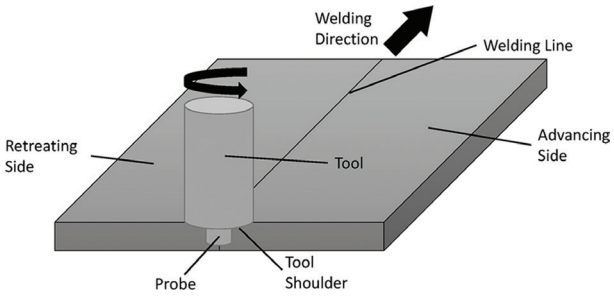

Figure 1. Scheme of friction stir welding process.

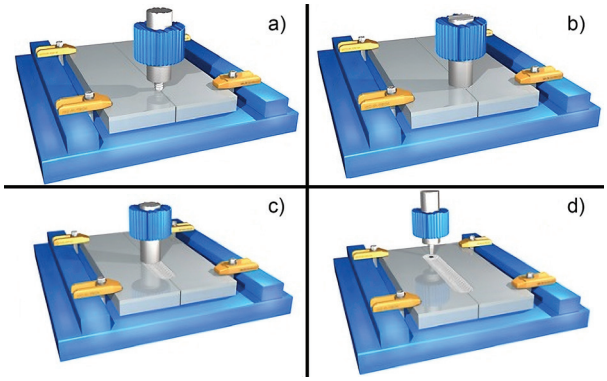

Figure 2. Scheme of FSW process steps: (a) rotating tool before plunging, (b) plunging and then tool shoulder touches the work piece surface producing frictional heat, (c) rotating tool traverses along the work piece and (d) pulling out from the workpiece.

The tool (**Figure 1**) has two main functions: heat the workpiece and move the material to produce the joint. The heat is produced mainly by the shoulder friction with the top surface of the workpiece. This softens the material to be welded. Moreover, the shoulder prevents expulsion of the material and guides the flow of the material during welding. The tool pin, in addition to being the secondary source of heat generation, provides the stirring action to the materials of the two plates to be joined [1]. FSW is mainly a mechanical process, and the forces involved in this type of work are relevant. Thus, the workpiece is placed on a thick backing plate and is clamped rigidly by strong fixture to eliminate any degrees of freedom.

2.2. Welding parameters

Two are the main parameters in FSW: tool rotation rate [rpm] and tool traverse speed [mm/min]. The rotation of tool controls the stirring and mixing action of the material, and the tool translation moves the stirred material from the front to the back of the pin. Higher tool rotation rates generate an increase of temperature due of higher friction heating and result in more intense stirring and mixing of material, but the frictional coupling of tool surface with

workpiece controls and governs the heating. Consequently, there is not a monotonic increase in heating with increasing tool rotation rate because the coefficient of friction at interface will change with the tool rotation rate.

Further, the insertion depth of pin into the workpieces (in position control mode) or the downward force on the tool (in force control mode) is important for producing good welds. When these parameters are not correct, the shoulder of tool may not contact the workpiece surface or create excessive flash around the welds.

In addition, preheating or cooling can also be important for some FSW processes. For example, in materials with high melting point such as steel or titanium, the heat produced by friction and stirring may be not sufficient to soften and plasticize the material around the tool. In these cases, preheating or an additional external heating source, e.g. laser, can help the material flow and widen the process window [1].

2.3. Laser-assisted friction stir welding

In this technique, a defocused laser beam precedes the FSW tool during welding at a distance between 10 and 40 mm, increasing the temperatures reached in front of the tool and allowing an easier advancement of the same. In **Figure 3**, a scheme of the LAFSW setup has been reported.

The commonly used laser sources are diode laser, Nd:YAG fibre optic laser and CO_2 laser. The laser spot is activated just before the plunging stage or at the start of the welding phase of FSW [7]. The assistance of the laser in FSW is an attractive way to preheat the material with a conventional FSW setup. This technique has been employed to weld a variety of light alloys, high-strength alloys and dissimilar alloys. The higher heat input allows a better material plasticisation and grain refinements that improve the material flow and the mechanical properties. The better plasticisation should help also to reduce the downward axial force, the tool wear and increase welding speed [7].

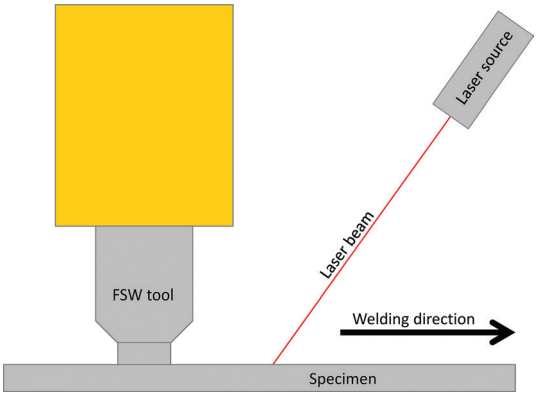

Figure 3. Scheme of the LAFSW setup.

http://dx.doi.org/10.5772/intechopen.72271

3. Temperature field in FSW and laser-assisted FSW processes

The temperature distributions and the thermal histories have a key role in FSW and LAFSW. They determine whether the welding process will produce a good weld, influencing the residual stresses, the microstructure and the strength of welds. Several studies have measured temperatures in FSW using thermocouples [8–10], but only a few have been involved in experimental analysis using thermography [9] and still less on laser-assisted friction stir welding. Employing thermocouples, Xu et al. [8] showed that the temperature decreases with decreasing the transverse speed and increases with increasing the rotational speed. Moreover, they noted that the distribution of the temperatures in the plunge phase is correlated only to the rotational tool speed. Finally, they showed that mechanical properties such as the yield and tensile strengths of the welded plate are related to the process parameters. Increasing the rotational tool speed increases yield and tensile strengths, while the elongation decreases. Hwang et al. [9] conducted a study on temperature distribution using thermocouples and find out that the temperatures on the advancing side are slightly higher than those on the retreating side. Also, Maeda et al. [10] have applied thermocouples on both top and bottom surfaces of the work plates and have found an asymmetric temperature distribution between the advancing side and the retreating side.

Although experimental measures are fundamental to understand the thermal phenomenon in the FSW process and LAFSW, they present some limitations, (e.g. economic costs or internal temperature measurements). For this reason, the implementation of numerical models that can predict the temperature distributions has a significant role to estimate the correct weld parameters, to improve mechanical properties of the welded joints and reduce the amount of trials and errors.

In the next section, the experimental setup employed to measure the temperature field on both FSW and LAFSW will be described. These experiments will be used for the validation of the numerical models that will be described later.

3.1. Thermographic analysis of FSW and laser-assisted FSW

A NEC H2640 infrared camera with configurable ranges between −40 and 2000°C, a resolution of 0.06°C, an accuracy of ±2°C and a spectral range of 8–13 μm has been used to acquire the temperature during the welding process. **Figure 4** shows the experimental setup of the thermal camera.

The angle between the FSW tool axis and the camera has been set to 30°. In order to reduce problems related to the low emissivity of aluminium and reflection, the specimen has been painted with matte black acrylic spray paint. An emissivity $\varepsilon = 0.95$ has been set on the camera.

When the specimens have to be mechanically tested after the welding process, the central zone of the specimen has not been painted to avoid paint inclusion into the welded joint. This allows to acquire correctly the temperature near the tool, but not influencing the mechanical characteristics of the joints. However, when there is the necessity to acquire the temperatures in front of the tool, e.g. in LAFSW, the specimens have been completely painted, and bead-on-plate welds have been done. Consequently, no mechanical tests have been done on this typology

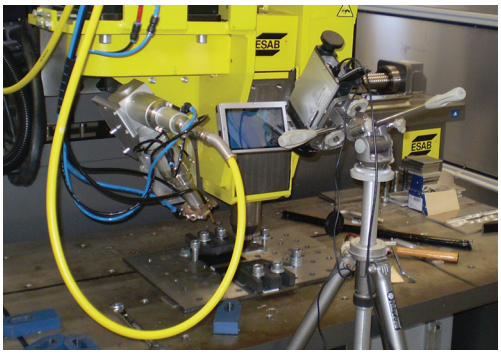

Figure 4. Thermographic experimental setup.

of specimens. Temperature measurements have been carried out on the retreating side of the welded plate because the configuration of the FSW machine prevents access to both sides.

3.2. Numerical prediction of temperature fields in FSW and LAFSW

3.2.1. FSW model description

Finite element analysis, by means of software ANSYS 14.5, has been implemented to develop a 3D transient thermal model and simulate the FSW thermal history. Due to the symmetry of the problem, a half plate model has been simulated to decrease the element number and reduce the computational time. The model has been meshed using 6000 SOLID90 elements. A thicker mesh has been employed near the welding line (**Figure 5**) to describe in a more accurate way the thermal behaviour near the tool area and to consider the higher gradient of temperature. The natural convection on the top surface and on the lateral side of the specimen has been set to 20 W/m^2 °C. Moreover, a convection coefficient of 300 W/m^2 °C has been employed to simulate the conduction between the backing plate and bottom surface of the specimen. The specific value of the convection coefficient has been employed to match the maximum temperature, reached during the weld process, between the experimental data and the numerical model.

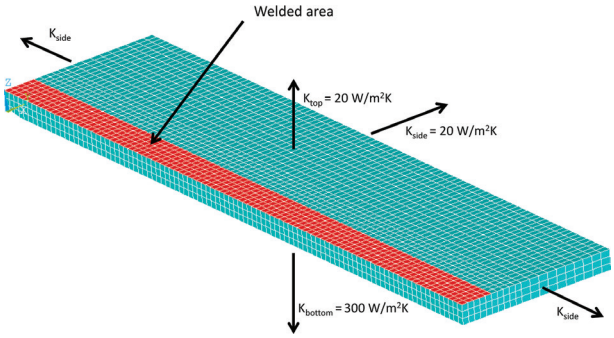

Figure 5. FSW model mesh and convection coefficient.

In the numerical model, as the temperature does not exceed 500°C, the heat lost by radiation has not been considered [11].

The AA5754 thermo-physical material properties (i.e. thermal conductivity and specific heat) have been implemented as a function of temperature [12]. Due to a lack of literature data, the density of the material has been kept constant with the temperature.

The welding process has been simulated by a moving thermal source along the welded zone. According to Schmidt et al. [13, 14], the analytical expression used for simulating FSW tool heat generation is reported in Eq. (1):

$$Q = \frac{2}{3}\mu\omega\frac{F_n}{R_{shoulder}^2}\left(\left(R_{shoulder}^3 - R_{probe}^3\right)(1+\tan\alpha) + R_{probe}^3 + 3\,R_{probe}^2\,H_{probe}\right) \quad (1)$$

The R_{probe} and $R_{shoulder}$ are the pin and shoulder radius of the tool (Eq. (1), **Figure 6**). H_{probe} and α are the pin height and the shoulder concavity angle. Moreover, F_n, ω and μ are the normal plunge force, the rotational speed and the friction coefficient, respectively. The μ coefficient has been set to 0.3 according with Schmidt et al. papers [13, 14]. The remaining terms in the equation are $R_{shoulder}$ 10.75 mm, R_{probe} 3 mm, $\alpha = 0°$ and H_{probe} 5.8 mm. The traverse speed has been set to 20 cm/min, the rotational speed to 500 RPM and the normal force F_n to 20,000 N in accordance with the process parameters.

3.2.2. Results and discussion for FSW model

The verification and validation of the previously described FSW model have been carried out on bead-on-plate welds. The studies have been regarded three steps (**Figure 7**) of the welding process. During each step, the numerical and experimental temperature data have been acquired and compared. In particular, the start phase is the welding initial step where the

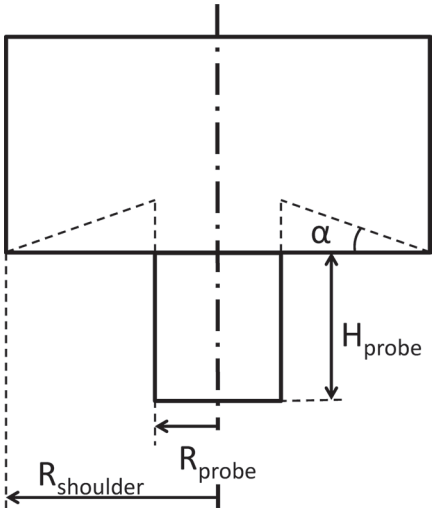

Figure 6. Tool geometry scheme.

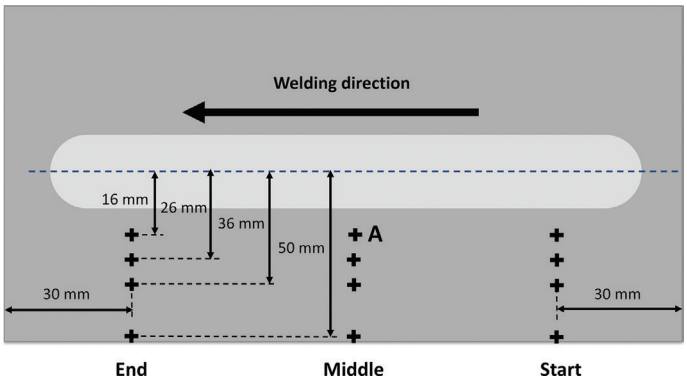

Figure 7. Location scheme of experimental measured points.

FSW tool is at about 30 mm from the edge of the plate. The middle step is in the half of the specimen, and finally, the end phase is at 30 mm from the left edge of the plate.

The graphs of the maximum temperatures versus distance from the weld line, for both experimental and numerical data, have been plotted in **Figure 8a–c**. The trends highlight that the estimation of the numerical model agrees with the experimental data. Indeed, in the start phase (**Figure 8a**), the maximum error between experimental and numerical data is 5.9%; in the middle step, it is 6.2% (**Figure 8b**) and in the end step (**Figure 8c**), the error is 6.3%. In order to accurately validate the numerical model, in **Figure 8d**, the temperature vs. time of the numerical model and experimental data for the point A in **Figure 7** has been reported. The trends are in good agreement though there are some small differences in the cooling phase. These differences are due to the use of heat convection instead of conduction in the numerical simulation of the contact between backing plate and specimen. Finally, the model is validated, and its results are good (37.1% of maximum error) considering all the parameters, such as coefficient of convection, friction coefficient and variability of normal force, that are difficult to consider.

Figure 9 shows the comparison between the numerical isothermals at the top surface of the specimen and the image of the surface temperature distribution taken by the infrared camera.

The white area in this figure describes the zone of the plate where the temperature exceeds 250°C. Overall, there is a good agreement between the numerical and experimental data on the whole plate. Only in the area near the clamping system, not implemented in the FEM model, the surface temperature is slightly different.

3.2.3. Laser-assisted FSW model description

The LAFSW numerical simulation is based on the previously described FSW model. However, beyond the adding of the laser source, some other improvements have been done, e.g. the adding of a backing plate to simulate in a better way the cooling phase. The same temperature-dependent thermo-physical properties of the previously described model have been

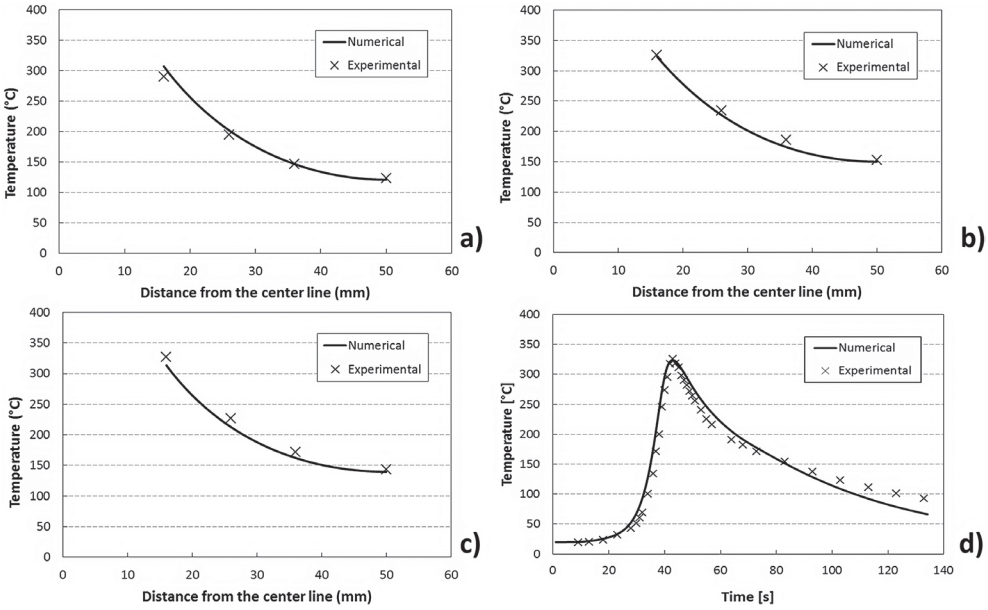

Figure 8. Temperature trend in the start phase (a), in the middle phase (b) and in the end phase (c) and temperature vs. time of a middle point distant 16 mm from the centre line (d) for FSW.

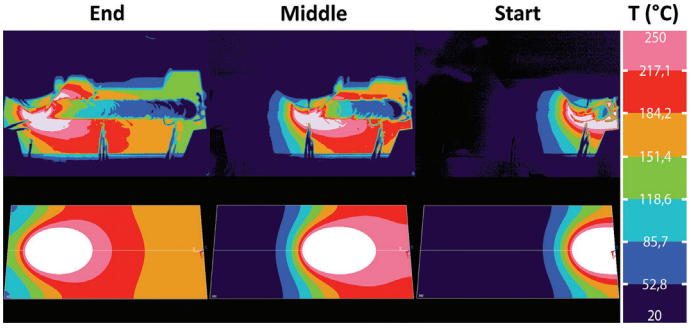

Figure 9. Graphical comparison between numerical data and the experimental ones for FSW.

used [12], and also in this case, only half plate has been simulated to reduce the computational time. The process parameters for the FSW are the same of the previous models. The laser power has been set to 500 W, and the distance of FSW tool-laser spot is 40 mm. A gradual thicker mesh of SOLID90 elements has been adopted near the welding line to describe more accurately the thermal behaviour where the temperature gradient is higher (**Figure 10**). The natural convection between aluminium and air has been set to 20 W/m^2 °C on the top surface and on the lateral side of the specimen. In this model, in different manners of the previous model, the interface between the backing plate and the specimen has been simulated

employing the conduction (**Figure 10**). A coefficient of 450 W/m^2 °C has been used to simulate the conduction between the backing plate (a 400 mm × 400 mm × 10 mm FE360 steel plate) and bottom surface of the specimen. The specific value of the conduction coefficient has been employed to match the maximum temperature, reached during the weld process, between the experimental data and the numerical model.

As in the previous FSW model, the welding process has been modelled as a uniform thermal source. However, while F_n is the same as the previous model, the friction coefficient μ has been set equal to 0.237 according to the experimental tests. Finally, the laser source has been simulated as a uniform heat source of 2 mm radius that moves together to FSW tool.

3.2.4. Result and discussion for laser-assisted FSW model

As in the previously shown results for FSW, also in this case, three different steps have been studied and reported in the later graphs. As in the previous model, the middle step is in the middle of the plate; instead, the start position and the end position are at 65 mm from the right and left plate edges, respectively. The temperature has been acquired at 16, 26, 36 and 50 mm from the welding line for each of the three steps. The trends of the temperature versus distance from the weld line have been plotted for numerical and experimental data in the start (**Figure 11a**), middle (**Figure 11b**) and end (**Figure 11c**) phases. Generally, these graphs show that the numerical model fits the experimental data with low errors. This is confirmed by R^2 value that is 0.992 in the start step, 0.999 in the middle phase and, finally, 0.999 in the end step. In **Figure 10d**, the temperature versus time of the experimental data and the numerical model has been reported. This graph represents the temperatures of a central point distant 16 mm from the welding line. In general, there is a good agreement between the numerical model and the experimental data, and compared to the previous model, the adding of the baking plate improves the cooling phase prediction (**Figure 8d** vs. **Figure 11d**).

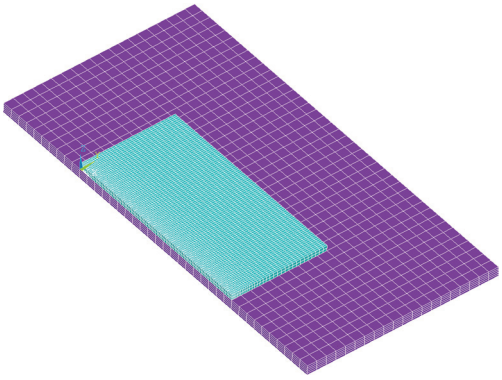

Figure 10. LAFSW scheme of model mesh.

http://dx.doi.org/10.5772/intechopen.72271

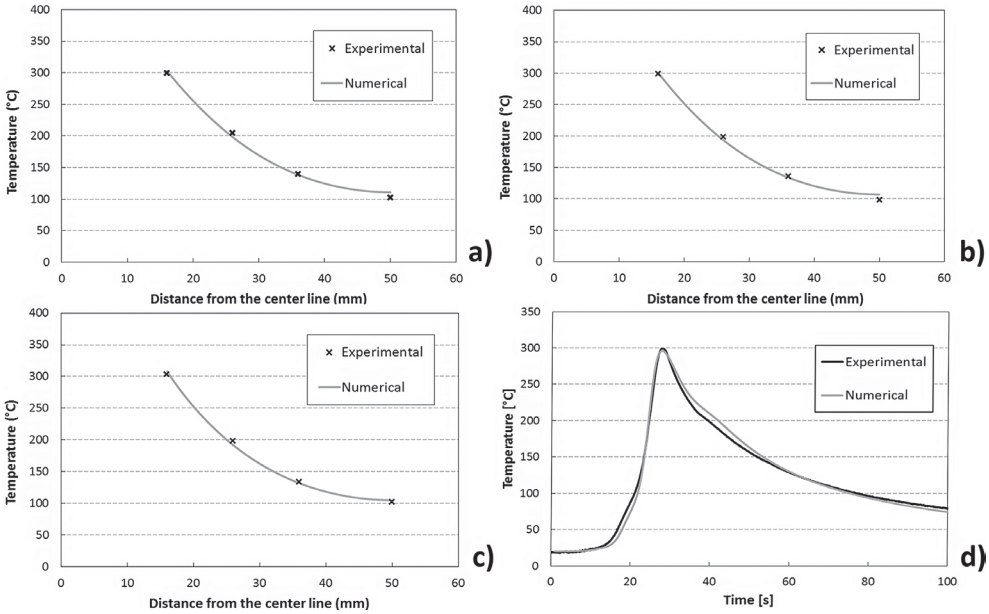

Figure 11. Temperature trend in the start phase (a), in the middle phase (b) and in the end phase (c) and temperature vs. time of a middle point distant 16 mm from the centre line (d) for LAFSW.

The value of the thermal contact conductance coefficient, between the aluminium specimens and the backing plate, has been selected to fit the numerical maximum temperature in the point A with the experimental data.

In **Figure 12**, a qualitative comparison of thermal field measured experimentally and that obtained numerically has been reported. Moreover, the temperature of welded area behind the FSW tool is not correct because there is a variation of the emissivity due to the paint removal and change of roughness after the transit of FSW tool.

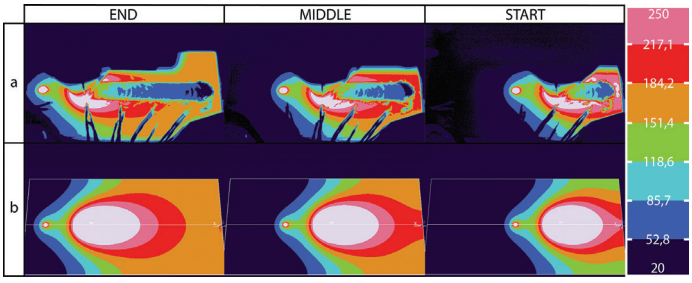

Figure 12. Graphical comparison between the experimental data (a) and numerical results (b) for LAFSW.

4. Residual stresses in FSW and LAFSW processes

Residual stresses have a fundamental role in welded structures because they affect the mechanical response of parts (i.e. corrosion resistance, fatigue life and many other material characteristics). Residual stress distribution, also in FSW process where, though the heat input is lower than traditional welding techniques, the constraints applied to the parts to weld are more severe, should be deeply studied.

Technical literature reports numerous research papers that deal with the experimental evaluation of residual stress distribution in FSW joints. Dalle Donne et al. [15], employing different techniques, have measured residual stress distribution on FSW 2024Al-T3 and 6013Al-T6 joints. They have shown that longitudinal and transverse residual stresses have a "M"-like distribution across the weld. Moreover, the longitudinal residual stresses are higher than the transverse ones regardless on traverse speed, tool rotation speed and pin diameter. Peel et al. [3], employing synchrotron X-ray method, have measured the residual stress in FSW AA5083 welded joints. The results show that there is a tension state in the weld bead in both longitudinal and transverse residual stress directions. Furthermore, they have proven that the longitudinal stresses increase with increasing the traverse speed. Sutton et al. [16] and also Donne et al. have proven that the longitudinal is the most important component in the residual stresses analysis in FSW process and that the transverse is about 70% of the longitudinal component.

In order to have a wider understanding of the FSW process, some researchers have recently simulated the FSW process by numerical models. Moreover, these numerical models have also the aim to develop the process through the research of optimal parameters minimising the amount of trial and error. Khandkar et al. [17] have made an uncoupled thermomechanical model for some aluminium alloys and 304 L stainless steel based on torque input for calculating temperature and then residual stress. Chen et al. [18] have developed a 3D numerical model to study the thermal impact and evolution of the residual stresses in the welded joints. However, the previously described numerical simulations are only thermal or thermomechanical models in which, for example, the tool mechanical force is not considered. These effects are important and should be included into the thermomechanical simulations.

Though many works on measuring residual stresses in FSW have been done, few works have been carried out on measuring or simulating residual stresses in innovative techniques, such as LAFSW. In the next section, the measurement of residual stresses in FSW and LAFSW will be presented, and the results will be useful to validate the FSW and LAFSW numerical models.

4.1. Residual stress measurements in FSW and LAFSW

FSW and LAFSW tests were conducted on 6-mm thick 5754 H111 aluminium alloy plates, in butt joint configuration. Two rectangular plates, 200 mm × 100 mm, have been welded perpendicular to the rolling direction. The welding process is the same in the previous sections.

A Xstress 3000 G3R Stresstech X-ray diffractometer has been employed to measure the residual stresses. 30 kV and 8 mA of current have been used to power a Cr tube ($\lambda = 0.2291$ nm). An angle of 156.7° has been selected as 2θ diffraction angle, and five ϕ different angles (0, ±22.5, ±45°) with an oscillation of ±3° have been employed to increase the quality of the measures. The residual stresses, both longitudinal (x-axis direction) and transverse (y-axis direction), have been carried out along the centre line of the specimens, i.e. the line normal to the welding line in the middle of the plate.

4.2. Numerical prediction of residual stresses in FSW

4.2.1. Numerical model description

An uncoupled FE model has been carried out to calculate residual stress field. The first step has been to carry out a thermal analysis to simulate the temperature history related to the welding process. Then, the calculated temperature field has been used as thermal input to the mechanical model to predict the residual stresses and strains. This analysis has been implemented by means of FE software ANSYS 14.5. The thermal simulation is based on the previously presented model modified to describe the welding process of two 200 mm × 100 mm plates in butt-weld configuration. With the aim of an accurate simulation of residual thermal stresses, beyond the temperature-dependent thermophysical properties, also temperature-dependent thermomechanical properties have been used [13]. It is worth noting that enthalpy values are not considered in the simulation, as the FSW is a solid-state welding method and there is no material melting. Moreover, a multilinear isotropic hardening has been employed to describe the material behaviour.

In order to calculate the residual stresses, the thermal histories simulated by the FE thermal model have been inputted in the mechanical simulation. To this aim, the SOLID186 elements have been employed instead of the SOLID90 elements, keeping the same load step and mesh size. Moreover, to simulate the mechanical effect due to the compression force applied by the tool, a uniform axial pressure distributed on tool area has been included in the FE mechanical model. The mechanical constrains have been set according with experimental setup. Once that the welding simulation is concluded, the constraints are gradually released, and the residual stresses due to FSW process have been evaluated.

The FSW has been carried out perpendicular to the rolling direction of the AA5754 sheets. As the layout of the FSW machine does not allow an easy access to both side of the plate, the temperature measurement, residual stresses analysis and numerical simulation have been executed in the retreating side of the plate.

4.2.2. Results and discussion

Numerical model has been validated on both temperatures and stresses on the actual case in order to obtain reliable stress values in the simulated case. To reach this aim, the temperature field of the specimen has been measured during the FSW test by an infrared thermo-camera. In the same way, as in the Section 3.2.2, the recorded values have been compared with the data calculated by the numerical model in three different positions when maximum. The middle

step is in the half of the plate; instead, the start position and the end position are at 50 mm from the right and left plate edges, respectively. The temperature has been acquired at 16, 36, 80 and 100 mm from the welding line for each of the three steps. In **Figure 13**, the graphs of the temperature versus distance from the weld line have been plotted both for numerical and experimental data. Generally, the numerical results show a good agreement with the experimental measurements. This is confirmed by R^2 that is 0.997 in the start step (**Figure 13a**), 0.999 in the middle phase (**Figure 13b**) and, finally, 0.991 in the end step (**Figure 13c**). The graph of temperature vs. time for both experimental and numerical data (of the A point in **Figure 7**) has been reported in **Figure 13d**. In general, the trends of experimental and the numerical data are in good agreement with some small difference in the cooling phase as already explained previously.

The mechanical part of the model has been validated based on the X-ray diffraction stress-measured data. In **Figure 14** the stress in the welding direction, i.e. the longitudinal stress, has been reported and compared with the numerical values. The longitudinal stress shows a "M"-like distribution across the weld, and moreover, the maximum stress value in a FSW weld is located on the edge of the bead described in **Figure 14** by the vertical grey line at 10.75 mm from the welding line.

The residual stresses in the transverse direction, for both experimental and numerical data, have been reported in **Figure 15**. The transverse residual stress values are roughly constant in the plate with a value of 60 MPa and, in agreement with Sutton et al. [16], are about 70% of the longitudinal one.

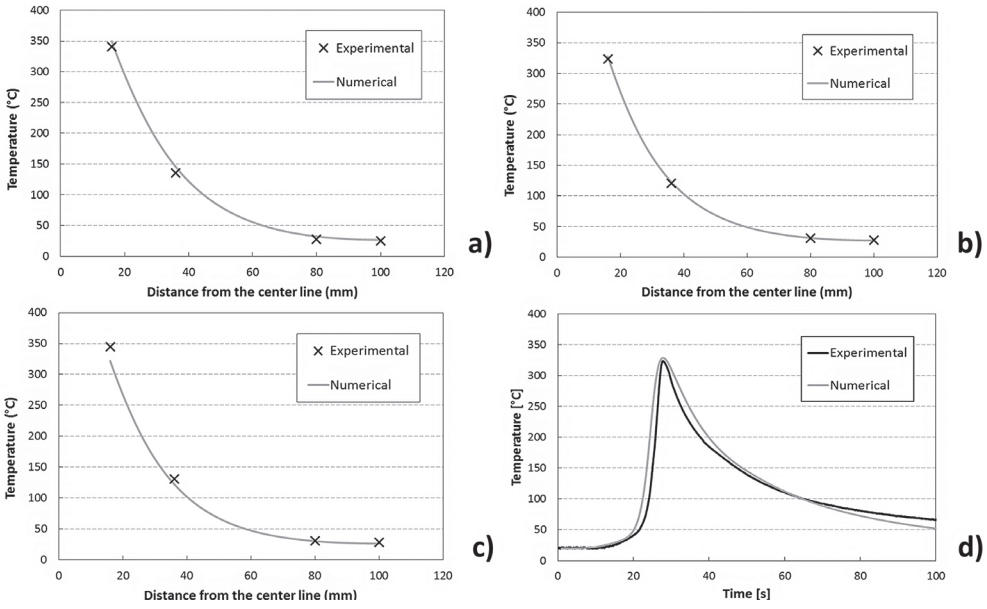

Figure 13. Temperature trend in the start phase (a), in the middle phase (b) and in the end phase (c) and temperature vs. time of a middle point distant 16 mm from the centre line (d) for FSW.

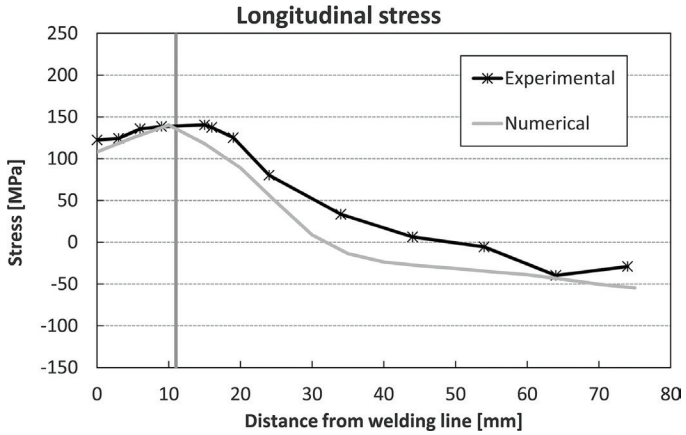

Figure 14. Numerical vs. experimental comparison of longitudinal stress in FSW.

The residual stress results show a good agreement between experimental and numerical data, although some little discrepancies exist. These are located away from the welding line where the initial residual stresses of the plate are preponderant. In the numerical model, the initial state of the plate is difficult to consider and to simulate.

4.3. Numerical prediction of residual stresses in LAFSW

4.3.1. Numerical model description

The mechanical part of the LAFSW model is based on the thermal model described in Section 3.2.3, but to the previously described thermal model, it has been added the

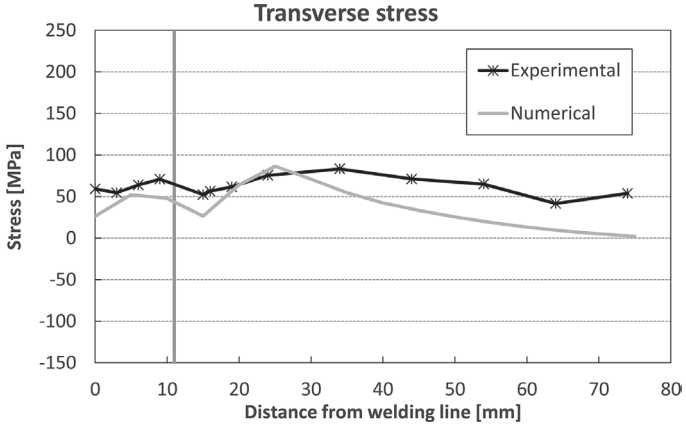

Figure 15. Numerical vs. experimental comparison of transverse stress in FSW.

mechanical part which employs the thermal data as an input to the mechanical model. However, as explained previously, the LAFSW has been validated on a bead-on-plate configuration to capture also the temperature in front of the tool. To validate the residual stress model, it is necessary to carry out the measurements on real butt-weld configuration. In order to solve this problem, once the numerical model has been validated (see Section 3.2.4), it has been implemented on the basis of the actual welding setup simulating the joining of two 200 mm × 100 mm plates. The new temperature distribution has been inputted to the mechanical part of the model to simulate the residual stresses in the actual configuration. Finally, the experimental data have been compared to the numerical residual stress values.

The same procedure to pass the temperature data from the thermal model to the mechanical part as an input, explained in Section 4.2.1, has been also employed in this model. Also in this case, the mechanical constrains have been set according to experimental setup, and once that the welding simulation is concluded, the constraints are gradually released, and the residual stresses due to LAFSW process have been evaluated.

4.3.2. Results and discussion

In **Figure 16**, the numerical versus experimental longitudinal stress trend has been reported for the retreating side. Also in this case, the maximum stress value in the LAFSW welds is located on the edge of the bead as has been shown in **Figure 16** by a vertical grey line at 10.75 mm from the joining line.

The transverse residual stress trend has been reported in **Figure 17**. This trend shows, for both experimental and numerical data, that the transverse residual stress values are roughly constant in the plate and that there is a good agreement between numerical and experimental results. However, the effect of the laser is visible in the welded zone where there is a small increment of the residual stress values.

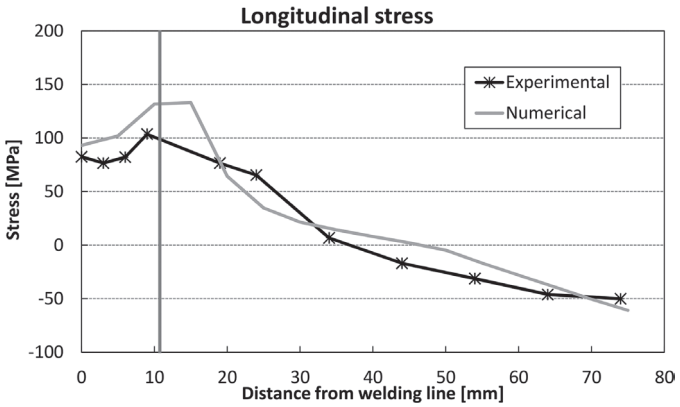

Figure 16. Numerical vs. experimental comparison of longitudinal stress for LAFSW.

http://dx.doi.org/10.5772/intechopen.72271

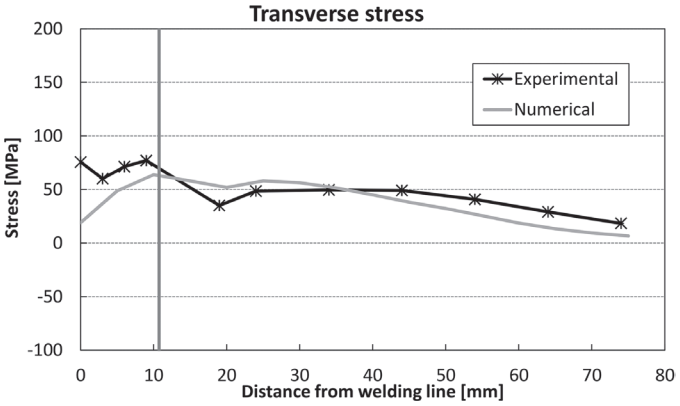

Figure 17. Numerical vs. experimental comparison of transverse stress for LAFSW.

5. Summary and conclusions

In this chapter, two 3D thermo-mechanical models have been developed in order to predict temperatures and residual stresses in friction stir welding and laser-assisted FSW. These models include the mechanical action of the shoulder and the thermo-mechanical characteristic of AA5754 at different temperatures. Thermographic analysis of FSW and LAFSW process and residual stress measurement by X-ray diffraction has been carried out to validate the model thermally and mechanically.

The results for both the numerical models and experimental data show that the longitudinal stress presents a "M"-like distribution across the weld, and moreover, the maximum stress value in a FSW and LAFSW weld is located on the edge of the bead. The stress in the transverse direction is roughly constant with values between 50 and 60 MPa along all the transverse directions of the plate. Moreover, according to the observations reported by Sutton et al. [16], the transverse stress has lower values than longitudinal stress and it is about 70% of the this one.

Although some little discrepancies exist between the simulated numerical values and the measured ones, the distribution of the residual stress, both longitudinal and transverse, shows a good agreement with the experimental results for both FSW and LAFSW models. However, away from the welding line, there is the maximum difference between numerical and experimental data for both longitudinal and transverse stresses. This could be explained considering that the initial residual stress in the numerical model is difficult to consider. Indeed, away from the welding line, the influence of the welding process is minimal, and the residual stress trend should tend to the pre-weld value.

In conclusion, the importance of the prediction and measurement of residual stress in FSW and LAFSW has been highlighted. Though the FSW is a solid-state welding process, the residual stresses are not low in general, and the influence of these stresses on the mechanical behaviour of the FSW joints should be considered.

As a future development of this work, the authors are improving the described models and Eq. (1) to consider and predict the differences in the temperatures and, thus, in the residual stresses between advancing and retreating sides. These differences change in accordance to the traverse and the rotating tool speeds due to the concordance and discordance between the travel and the rotating tool directions in, respectively, the advancing and the retreating sides.

Author details

Caterina Casavola*, Alberto Cazzato and Vincenzo Moramarco

*Address all correspondence to: casavola@poliba.it

Department of Mechanics, Mathematics and Management, Polytechnic University of Bari, Bari, Italy

References

[1] Mishra RS, Ma ZY. Friction stir welding and processing. Materials Science and Engineering: R: Reports. 2005;**50**(1-2):1-78

[2] Reynolds AP, Tang W, Gnaupel-Herold T, Prask H. Structure, properties, and residual stress of 304L stainless steel friction stir welds. Scripta Materialia. 2003;**48**(9):1289-1294

[3] Peel M, Steuwer A, Preuss M, Withers PJ. Microstructure, mechanical properties and residual stresses as a function of welding speed in aluminium AA5083 friction stir welds. Acta Materialia. 2003;**51**(16):4791-4801

[4] Prime MB, Gnäupel-Herold T, Baumann JA, Lederich RJ, Bowden DM, Sebring RJ. Residual stress measurements in a thick, dissimilar aluminum alloy friction stir weld. Acta Materialia. 2006;**54**(15):4013-4021

[5] Darvazi AR, Iranmanesh M. Prediction of asymmetric transient temperature and longitudinal residual stress in friction stir welding of 304L stainless steel. Materials & Design. 2014;**55**:812-820

[6] Rhodes CG, Mahoney MW, Bingel WH, Spurling RA, Bampton CC. Effects of friction stir welding on microstructure of 7075 aluminum. Scripta Materialia. 1997;**36**(1):69-75

[7] Padhy G, Wu C, Gao S. Auxiliary energy assisted friction stir welding – Status review. Science and Technology of Welding and Joining. 2015;**20**(8):631-649

[8] Xu W, Liu J, Luan G, Dong C. Temperature evolution, microstructure and mechanical properties of friction stir welded thick 2219-O aluminum alloy joints. Materials & Design. 2009;**30**(6):1886-1893

[9] Hwang YM, Kang ZW, Chiou YC, Hsu HH. Experimental study on temperature distributions within the workpiece during friction stir welding of aluminum alloys. International Journal of Machine Tools and Manufacture. 2008;**48**(7-8):778-787

[10] Maedaa M, Liub H, Fujiib H, Shibayanagib T. Temperature field in the vicinity of FSW-tool during friction stir welding of Aluminium alloys. Welding in the World. 2005;**49**(3):69-75

[11] Chao YJ, Qi X, Tang W. Heat transfer in friction stir welding—Experimental and numerical studies. Journal of Manufacturing Science and Engineering. 2003;**125**(1):138-145

[12] Khanna SK, Long X, Porter WD, Wang H, Liu CK, Radovic M, Lara-Curzio E. Residual stresses in spot welded new generation aluminium alloys part A–thermophysical and thermomechanical properties of 6111 and 5754 aluminium alloys. Science and Technology of Welding & Joining. 2013;**10**(1):82-87

[13] Schmidt HB, Hattel JH. Thermal modelling of friction stir welding. Scripta Materialia. 2008;**58**(5):332-337

[14] Schmidt H, Hattel J, Wert J. An analytical model for the heat generation in friction stir welding. Modelling and Simulation in Materials Science and Engineering. 2004;**12**(1):143

[15] Dalle Donne C, Lima E, Wegener J, Pyzalla A, Buslaps T. Investigations on residual stresses in friction stir welds. In: 3rd International Symposium on Friction Stir Welding; 27-28 September 2001; Kobe (Japan). TWI, Cambridge (UK); 2001. pp. 1-10

[16] Sutton MA, Reynolds AP, Wang DQ, Hubbard CRA. Study of residual stresses and microstructure in 2024-T3 aluminum friction stir butt welds. Journal of Engineering Materials and Technology. 2002;**124**(2):215-221

[17] Khandkar MZH, Khan JA, Reynolds AP, Sutton MA. Predicting residual thermal stresses in friction stir welded metals. Journal of Materials Processing Technology. 2006;**174**(1):195-203

[18] Chen C, Kovacevic R. Finite element modeling of friction stir welding – Thermal and thermomechanical analysis. International Journal of Machine Tools and Manufacture. 2003;**43**(13):1319-1326